

Article

Effect of Clay Colloid Particles on Formaldehyde Transport in Unsaturated Porous Media

Theodosia V. Fountouli and Constantinos V. Chrysikopoulos * 

School of Environmental Engineering, Technical University of Crete, 73100 Chania, Greece; tfountouli@isc.tuc.gr

* Correspondence: cvc@enveng.tuc.gr

Received: 10 November 2020; Accepted: 14 December 2020; Published: 16 December 2020



Abstract: This study examines the effects of two representative colloid-sized clay particles (kaolinite, KGa-1b and montmorillonite, ST_x-1b) on the transport of formaldehyde (FA) in unsaturated porous media. The transport of FA was examined with and without the presence of clay particles under various flow rates and various levels of saturation in columns packed with quartz sand, under unsaturated conditions. The experimental results clearly suggested that the presence of clay particles retarded by up to ~23% the transport of FA in unsaturated packed columns. Derjaguin–Landau–Verwey–Overbeek (DLVO) interaction energy calculations demonstrated that permanent retention of clay colloids at air-water interfaces (AWI) and solid-water interfaces (SWI) was negligible, except for the pair (ST_x-1b)–SWI. The experimental results of this study showed that significant clay colloid retention occurred in the unsaturated column, especially at low flow rates. This deviation from DLVO predictions may be explained by the existence of additional non-DLVO forces (hydrophobic and capillary forces) that could be much stronger than van der Waals and double layer forces. The present study shows the important role of colloids, which may act as carriers of contaminants.

Keywords: unsaturated porous media; clay colloids; kaolinite; montmorillonite; formaldehyde; sand; co-transport

1. Introduction

Colloid-sized particles are in great abundance in unsaturated or vadose zones, and they are capable of binding a variety of contaminants. Colloid-sized particles either facilitate or hinder contaminant migration in the subsurface. Colloid particles are frequently mobilized in the vadose zone during infiltration events, which are initiated by rainfall, snowmelt or irrigation [1]. Therefore, a complete understanding of the role of colloids on contaminant transport in the subsurface is essential.

Many studies have focused on colloid and colloid facilitated contaminant transport in porous media [2–5]. Several studies have focused specifically on colloid transport in the presence of metals [6], pesticides [7,8], and pharmaceuticals [9–11]. Some other studies have examined the co-transport of colloids with bio-colloids experimentally [12–15], and numerically [16]. However, the majority of colloid transport studies are focused on fully saturated porous media [17,18]. Relatively little research has been conducted on the transport of colloids in the presence of contaminants under water-unsaturated conditions [19–22].

In unsaturated porous media, there exist three phases: solid, water and air. Consequently, there are numerous mechanisms that contribute to colloid mobilization. The degree of water saturation can affect colloid spreading [23], and important interactions can occur at the solid-water interfaces (SWI) and air–water interfaces (AWI) [24]. The existence of two different interfaces makes the transport of colloids more complicated, because colloids can also be captured at the AWI, and immobilized by film straining [25]. Colloid capturing at the AWI is an irreversible process [26,27]. However, mobilization of colloids can be enhanced during drainage or groundwater table fluctuations.

Kaolinite and montmorillonite are common aluminosilicate clay minerals, which at colloidal size ($<2\ \mu\text{m}$) are highly mobile in the subsurface [28]. These mobile clay colloids have high surface area and cation exchange ability. They have a strong affinity for a variety of contaminants and often serve as carriers of contaminants in aquatic systems [11,29]. Moreover, formaldehyde (FA) is often released into soil systems in order to inactivate or destroy pathogenic bacteria and fungi [30]. FA can pose a risk to public health if it is released in the environment, because it is a contaminant of concern in surface waters, aquifers, and agricultural lands. FA has relatively strong affinity for kaolinite colloid particles [30].

The objective of the present study was to investigate the influence of flow rate and water content on the mobilization of FA and clay colloids (kaolinite and montmorillonite) in unsaturated sandy media. Studies conducted in unsaturated soils are of special importance because they are more representative of natural infiltration conditions. Furthermore, the available information on the simultaneous transport of multiple contaminants in unsaturated porous media is limited. To our knowledge, the transport of FA in unsaturated porous media in the presence of clay colloids has not yet been investigated.

2. Materials and Methods

2.1. Formaldehyde (FA)

The FA ($>99\%$) used in this study was purchased from Sigma-Aldrich. A 1000 mg/L FA stock solution was prepared and stored in a darkroom at $4\ ^\circ\text{C}$. The solutions were prepared by dilution of the stock solution at pH 7. All experiments were conducted using FA with initial concentration of $C_0 = 2\ \text{mg/L}$.

For the determination of FA concentration, the Nash colorimetric method was employed [31], which has been widely used in a number of studies [32–34]. In brief, a volume of FA-containing solution is mixed with Nash reagent at a maximum concentration of 8 mg/L (1:1 *v/v*). Nash reagent reacts with FA to produce the yellow colored diacetyl dihydro-lutidin product. The resulting complex is measured at 412 nm with a UV-VIS Spectrophotometer (Shimadzu, Japan, UV-1900). Preparation of 100 mL Nash reagent was obtained by adding 15 g of ammonium acetate, 0.3 mL of acetic acid, and 0.2 mL of acetyl acetone in distilled deionized water (ddH_2O). The solution was subsequently stored in a dark bottle. Ultrapure water (Easypure II, Barstead, NH, USA, resistivity of $\sim 18.2\ \text{M}\Omega\cdot\text{cm}$ at $25\ ^\circ\text{C}$) was used for the preparation of all solutions. The detection limit for this colorimetric method was 0.17 mM [34]. All of the experiments with FA were performed in a fume hood.

2.2. Sand Packed Columns and Colloids

The columns were packed with quartz sand. The grain diameter of the quartz sand was in the range 0.425–0.600 mm (sieve No. 30/40). Metal oxides and trace quantities of organics present on the surface of sand may influence the surface characteristics of sand and may promote colloid deposition [24]. A solution containing 0.1 M HNO_3 (70%) and 0.1 M NaOH was used to wash the sand which was then rinsed thoroughly with ddH_2O [35,36]. Subsequently, the sand was dried at $80\ ^\circ\text{C}$ before storage in a sealed beaker until use.

The clay colloids Kaolinite (KGa-1b, well crystallized kaolin, from Washington County, Georgia) and Montmorillonite (ST_x -1b, Ca-rich montmorillonite, white, from Gonzales County, Texas) were purchased from Clay Minerals Society (Columbia, MO, USA). KGa-1b has a specific surface area (SSA) of $10.1\ \text{m}^2/\text{g}$, according to the Brunauer–Emmet–Teller (BET) method, and a cation exchange capacity (CEC) of 2.0 meq/100 g. ST_x -1b has respective SSA and CEC values of $82.9\ \text{m}^2/\text{g}$ and 84.4 meq/100 g, respectively. Only KGa-1b and ST_x -1b particles with size $<2\ \mu\text{m}$ separated by sedimentation [37] and purified according to Rong et al. [38] were used. Specifically, a quantity of 12.5 g of clay was mixed with 50 mL ddH_2O in a 1-L beaker and then 5–10 mL of a 30% hydrogen peroxide solution was added to oxidize the organic matter, while adjusting the pH to 10 with 0.1 M NaOH. After dilution of the suspension in a volume of 1 L, the colloid fraction with size $<2\ \mu\text{m}$ was separated from larger

particles by sedimentation (1 h). The separated suspension of colloids was flocculated using a 1 M NaCl solution. Finally, the separated colloid particles were washed thoroughly using ddH₂O and ethanol, and subsequently dried at 60 °C.

Clay particles (KGa-1b or ST_x-1b) in appropriate amounts were resuspended in ddH₂O. The suspensions were subsequently sonicated (37 kHz) for 15 min by an ultrasonic processor (Elmasonic S 30/(H), Elma Schmidbauer GmbH, Singen, Germany) to avoid aggregation. The initial concentration of the two clays (100 mg/L) was within the range of colloid concentrations measured in the vadose zone [39,40]. The resulting suspensions for all the experiments had a pH of 6.85 ± 0.05 . A ZetaSizer analyzer (Nano ZS90, Malvern Instruments) was used to measure the zeta potential and hydrodynamic diameter of the suspended clay colloids, which were -32.7 ± 2.6 mV and 1141 nm for KGa-1b particles, and -25.6 ± 4.6 mV and 1173 nm for ST_x-1b particles, respectively (see Table 1). All measurements were obtained in triplicate. The optical density of colloids was measured at 280 nm using a UV-vis Spectrophotometer (UV-1900, Shimadzu).

Table 1. Zeta potentials of clay colloids in the presence and absence of FA.

Zeta Potentials (mV)	
KGa-1b	-32.7 ± 2.6
ST _x -1b	-25.6 ± 4.6
KGa-1b & FA	-36.8 ± 5.8
ST _x -1b & FA	-37.8 ± 3.0

2.3. Column Transport Experiments

A cylindrical Plexiglas column with length of 15.2 cm and internal diameter of 2.6 cm was used for the column experiments. The unsaturated column setup used in this study (see Figure 1) was similar to the one employed by Anders and Chrysikopoulos [41], and Mitropoulou et al. [42]. The column was packed by adding quartz sand in small increments with gentle vibration of the column, using a pestle, in order to avoid formation of stratifying layers [43]. To ensure that the packed column was fully saturated without any trapped air bubbles, several pore volumes of ddH₂O were passed from the bottom to the top of the column at a flowrate of 1 mL/min. The porosity of each packed column was calculated gravimetrically and listed in Table 2. The observed range of porosities was 0.41–0.45.

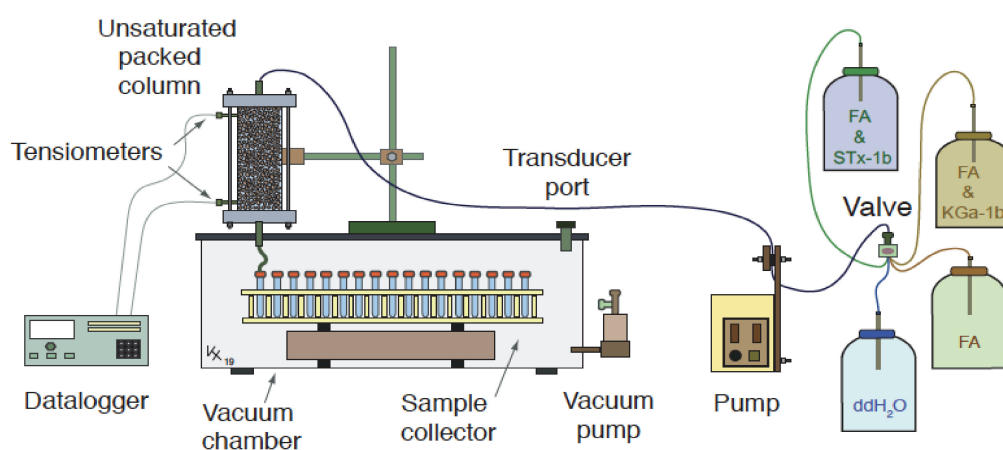


Figure 1. Schematic illustration of the experimental apparatus.

Table 2. Experimental conditions and results. †

Experiment	Flow Rate (mL/min)	S_w (%)	θ_m (-)	θ (-)	U (cm/min)	M_r (%)	$M_{1(i)}/M_{1(tr)}$ (-)	a_{exp} (-)	$(C/C_0)_{max}$ (-)
Formaldehyde (FA)	1	41.9	0.18	0.43	0.44	84.2	0.95	–	0.97
FA	1.5	50.0	0.22	0.44	0.65	89.0	1.04	–	0.98
FA	2	61.4	0.28	0.45	0.84	91.3	1.06	–	0.99
FA	3	70.7	0.31	0.44	1.29	85.9	1.02	–	1.00
FA-(KGa-1b)	1	40.9	0.18	0.44	0.43	67.6–44.3	(0.76)–(0.50)	0.129	(0.75)–(0.59)
FA-(KGa-1b)	1.5	52.4	0.23	0.43	0.66	62.6–66.8	(0.74)–(0.79)	0.021	(0.73)–(0.94)
FA-(KGa-1b)	2	59.0	0.25	0.42	0.89	64.7–64.1	(0.76)–(0.75)	0.065	(0.78)–(0.84)
FA-(KGa-1b)	3	70.0	0.30	0.43	1.31	72.4–82.8	(0.86)–(0.98)	0.009	(0.85)–(0.98)
FA-(ST _x -1b)	1	40.7	0.17	0.41	0.46	74.8–68.5	(0.85)–(0.77)	0.039	(0.88)–(0.84)
FA-(ST _x -1b)	1.5	50.1	0.21	0.41	0.68	69.7–74.1	(0.82)–(0.87)	0.035	(0.85)–(0.89)
FA-(ST _x -1b)	2	59.9	0.24	0.41	0.93	78.7–71.3	(0.92)–(0.83)	0.044	(0.94)–(0.89)
FA-(ST _x -1b)	3	70.2	0.29	0.41	1.38	74.5–80.2	(0.89)–(0.95)	0.001	(0.90)–(1.00)
Tracer	1	40.8	0.17	0.42	0.45	88.5	–	–	–
Tracer	1.5	49.5	0.21	0.42	0.67	84.8	–	–	–
Tracer	2	59.6	0.25	0.42	0.89	85.7	–	–	–
Tracer	3	70.0	0.30	0.42	1.34	84.1	–	–	–

† Where S_w is the degree of saturation, θ_m is the water content, θ is the porosity, U is the interstitial velocity, M_r is the mass recovery, a_{exp} is the collision efficiency, and $(C/C_0)_{max}$ is the maximum effluent concentration. The various initial concentrations are: $C_{0_FA} = 2$ mg/L, $C_{0_KGa-1b} = 100$ mg/L, $C_{0_STx-1b} = 100$ mg/L.

Because the pressure potential in unsaturated soil is always negative, a constant suction must be applied at the bottom of the column in order to extract the pore water and achieve unsaturated conditions. Therefore, the packed soil column was placed on top of a vacuum chamber so that the lower column outlet was positioned tightly in the conical shaped hole of the cover plate (Soil Measurement Systems, Tucson, AZ, USA). A fraction collector was positioned inside the vacuum chamber so that the column effluent drips directly into the test tube that needs to be filled. The vacuum in the chamber was adjusted using a pressure regulator, which was monitored by a hand-held tensiometer attached to the tensiometer port. The experiments were performed under a pressure difference of about 5 kpa. The input solution was applied to the top of the column, using a syringe pump. The column was equilibrated with several pore volumes of ddH₂O in order to achieve steady-state flow through the column. This was followed by ~6 pore volumes of an experimental solution containing FA or FA-colloids. Finally, the column was flushed with 2 pore volumes of ddH₂O. The effluent (9 mL) was collected in 10 mL glass tubes at regular time intervals.

Two tensiometers were applied at 2.5 and 7.5 cm from the upper sand surface to measure the water potential of the packed column. The experimental water potential data were acquired in real time from the tensiometers with a CR800 datalogger (Campbell Scientific, Inc., Logan, UT). The experiments were carried out at room temperature (~23 °C), and all additional experimental conditions are listed in Table 2.

Note that the water content in each packed column was adjusted by modifying the vacuum chamber pressure and the influent flowrate. The desired degree of saturation was achieved by draining the initially saturated column, and by changing the influent flowrate according to the hydraulic conductivity that corresponded to the specified saturation. At the bottom of the column, the pressure head was slowly dropped until practically equal measurements at the two tensiometers were observed.

Column transport experiments were conducted at four different flowrates (1, 1.5, 2 and 3 mL/min), resulting in four different levels of water saturation (~40, 50, 60, 70%, respectively). The volumetric water content (θ_m) and degree of saturation (S_w) were calculated gravimetrically by measuring the weight of the dry and wet column (initially and at the end of the experiment), and these are listed in Table 2. The volumetric water content is defined as the ratio of liquid volume to porous medium volume (L^3/L^3), and the degree of saturation ($S_w = \theta_m/\theta$) is measured as the ratio of the volumetric water content to porosity.

For each water-content, a tracer experiment was conducted in a fashion similar to the FA or FA-colloid transport experiments. Chloride anion, in the form of 5 mM sodium chloride (NaCl) was used as a soluble tracer [44]. The chloride concentration was measured by ion chromatography

(761 Compact IC, Metrohm, with a separator column Metrosep A Supp 4–250 × 4.0 mm). The tracer experimental conditions are listed in Table 2.

3. Theoretical Considerations

The concentrations of FA, FA-colloids, and tracer collected at the end of the packed column ($x = L$) were analyzed by the first absolute temporal moment, $M_1(t)$, which describes the mean residence time or average velocity [45]. The mass recovery, $M_r(-)$, of the injected FA or FA-colloid complex was quantified by the following equation [46]:

$$M_r = \frac{m_0}{M_{in}/U} \quad (1)$$

where m_0 ($t \cdot M/L^3$) is the total mass in the concentration breakthrough curve, M_{in} (M/L^2) is the mass injected in the column, and U (L/t) is the interstitial fluid velocity.

In this study, four different effluent concentrations were determined: (1) FA in the absence of clay colloids, C_{FA} (M/L^3), (2) clay colloids (kaolinite or montmorillonite), C_{cc} (M/L^3), (3) FA in the presence of clay colloids, C_{FA-cc} (M/L^3), and (4) tracer, C_{tr} (M/L^3). The mass recovery, $M_r(-)$, for each of the four different concentrations (C_{FA} , C_{cc} , C_{FA-cc} , and C_{tr}) was determined. Also, the temporal moments, $M_1(t)$, of the C_{FA} , C_{cc} , and C_{FA-cc} concentration distributions were normalized with that of C_{tr} . Note that M_1 describes the mean residence time or average velocity. Also, the ratio $M_{1(i)}/M_{1(tr)}$ compares the velocity of species “i” relative to that of the conservative tracer. Note that when $M_{1(i)}/M_{1(tr)} < 1$, there is solute or particle retardation and when $M_{1(i)}/M_{1(tr)} > 1$ there is solute or particle velocity enhancement.

The dimensionless collision efficiency, α_{exp} , was estimated using the equation [47]:

$$\alpha_{exp} = -\frac{2}{3} \frac{d_c}{L(1 - \theta_m)\eta_0} \ln \left[\frac{C_{iss}}{C_{i0}} \right] \quad (2)$$

where d_c (L) is the mean collector diameter, C_{iss} (M/L^3) is the effluent concentration of colloid i after the breakthrough curve has reached a steady state, C_{i0} (M/L^3) is the influent colloid concentration, and η_0 is the single collector contact efficiency. Here η_0 was calculated from the relationship provided by Tufenkji and Elimelech [48] by replacing θ with θ_m and using the following parameter values: particle diameter for kaolinite $d_p = 1141$ nm, particle diameter for montmorillonite $d_p = 1173$ nm, particle density for clay colloids $\rho_p = 2200$ kg/m³ [49], fluid density $\rho_f = 999.7$ kg/m³, Boltzman constant $k_B = 1.38 \times 10^{-23}$ (J/K), Hamaker constant $A_{123} = 7.5 \times 10^{-21}$ J for the colloid water sand interaction [13], absolute temperature $T = 298$ K, dynamic fluid viscosity $\mu_w = 8.91 \times 10^{-4}$ kg/(m·s), and gravitational acceleration $g = 9.81$ m/s².

The total interaction energy, Φ_{DLVO} (J), between clay colloid–SWI and clay colloid–AWI were calculated based on the classical Derjaguin–Landau–Verwey–Overbeek (DLVO) theory using the following expression [50–53]:

$$\Phi_{DLVO}(h) = \Phi_{vdW}(h) + \Phi_{dl}(h) + \Phi_{Born}(h) \quad (3)$$

where Φ_{vdW} (J) is the van der Waals energy estimated by the expression provided by Gregory [54], Φ_{dl} (J) is the electrostatic interaction energy estimated by the expression provided by Hogg et al. [52], Φ_{Born} (J), is the Born interaction energy estimated by the expression reported by Ruckenstein and Prieve [55], and h [m] is the separation distance between two approaching areas. For both colloid–SWI and colloid–AWI systems, the ideal sphere–plate model was employed.

The combined Hamaker constant, A_{123} , defined by Israelachvili [56], was estimated by the procedures outlined by Syngouna and Chrysikopoulos [50], using previously measured values of A_{121} equal to 3.1×10^{-20} J for kaolinite, and 2.5×10^{-20} J for montmorillonite [57], $A_{22} = 3.7 \times 10^{-20}$ J and $A_{33} = 0$ J [56]. Furthermore, the calculated A_{11} was equal to 1.36×10^{-19} J for kaolinite, and 1.23×10^{-19} J for montmorillonite, the calculated A_{123} for colloid–water–AWI system was equal to -3.39×10^{-20} J for

kaolinite and -3.05×10^{-20} J for montmorillonite, whereas the value of A_{123} for colloid-water-SWI was set equal to 7.5×10^{-21} J for both clay colloids. The negative values of the Hamaker constants for clay colloids indicate that the van der Waals forces are repulsive for clay colloids at the AWI, whereas positive values imply that the van der Waals forces are attractive for clay colloids at the SWI.

Although natural colloids are not spherical, often they are assumed to be spherical particles, in order to calculate the various forces that act upon them [58]. Within unsaturated soil pores there exist capillary forces, which strongly affect water distribution, as well as flow and transport [59]. Colloid capillary retention represents the deposition of colloids in unsaturated porous media through capillary force interactions. Certainly, the capillary and associated friction forces are instrumental to colloid retention within water films [59]. At low water contents, capillary forces pin the colloid to the sand surface [58].

A capillary force, F_c ($M \cdot L/t^2$), acting on a colloid captured in a thin water film, developed around a sand grain, can be decomposed into two forces: one parallel, F_{pc} ($M \cdot L/t^2$), and one vertical F_{vc} ($M \cdot L/t^2$) to the sand surface. The force components parallel to the sand grain (laterally around the colloid) are balanced so that the net force is equal to zero, and the vertical forces can be combined into one force through the center of the colloid, which holds the colloid against the sand surface. Note that the grain surface is assumed to be flat, because the diameter of the clay used in this study is much smaller than the diameter of a sand grain. The expression required for the calculation of the total vertical capillary force, F_{v-tot} , for a spherical colloid with radius r_p (L), trapped to the grain surface within a water film with height h_f , has been provided by Bai et al. for the case where $h_f \leq 2r_p$ [60]. The capillary potential energy, Φ_C (J), for a colloid that protrudes a distance, d_f , out of the film or the air–water–solid interface, was calculated using the expression provided by Gao et al. [59], with the following contact angles $\beta_{KGa-1b} = 46.1^\circ$ and $\beta_{STX-1} = 30.5^\circ$ [61].

4. Results and Discussion

4.1. Transport Experiments

Figure 2 presents the normalized effluent FA concentrations (C/C_0) as function of pore volume for the transport experiments in water unsaturated columns packed with sand, at 4 different flow rates (1, 1.5, 2, and 3 mL/min). For comparison purposes, together with the FA breakthrough data are shown the corresponding conservative tracer (chloride) breakthrough curves. Note that the tracer breakthrough curves are approximately symmetric in shape, indicating that physical non-equilibrium is not significant, due to a narrow pore size distribution of the sand. The very small concentration fluctuations observed are attributed to experimental errors associated with concentration measurements and small variations in water flux. Note that the maximum normalized FA concentrations ($(C/C_0)_{max}$) in the effluent were practically equal to 1.0 for all flow rates examined (see Table 2). The FA breakthrough curves for all flow rates were also practically identical to the corresponding breakthrough curves of the conservative tracer. This observation suggests that there was no significant interaction between FA and the sand or the air-water interfaces in the unsaturated columns (see Figure 2). Note that Fountouli et al. [32] have also reported the absence of FA retention by the quartz sand in batch and water saturated packed columns.

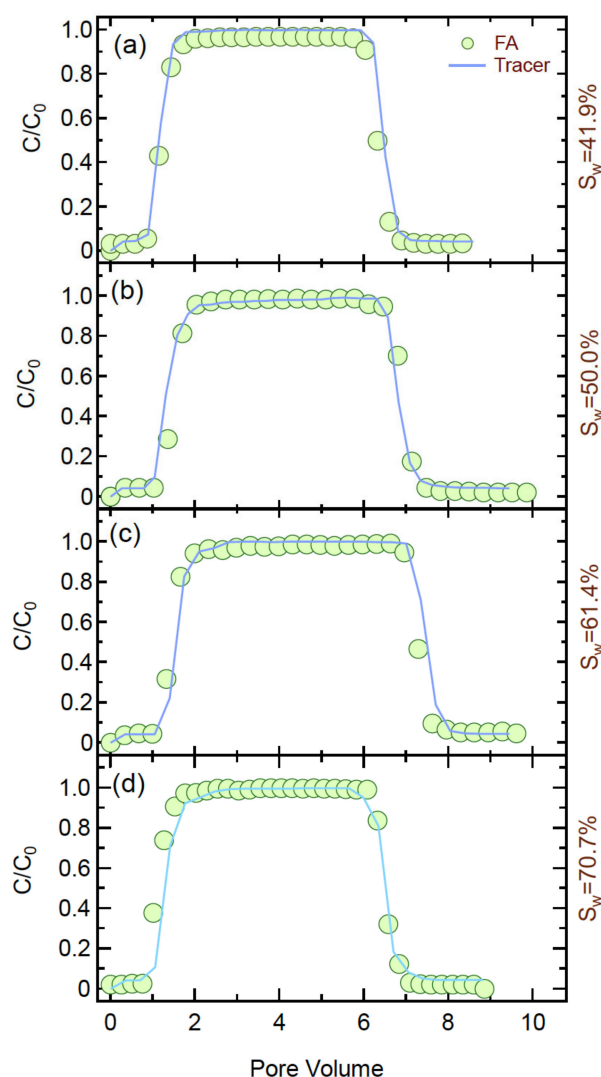


Figure 2. Breakthrough data from the transport experiments with FA and tracer in unsaturated columns packed with sand under various flow rates: (a) 1, (b) 1.5, (c) 2, and (d) 3 mL/min.

Furthermore, for each breakthrough curve, the M_r values, as calculated with Equation (2), and the ratio of M_1 for FA to that for tracer ($M_{1(\text{FA})}/M_{1(\text{tr})}$) were computed and listed in Table 2. The mass recoveries and peak concentrations for FA with increasing flow rate and increasing saturation level, S_w (-), remained practically steady. As expected, the ratio $M_{1(i)}/M_{1(\text{tr})}$, for all flow rates examined, is approximately equal to unity, suggesting that the transport of FA was neither retarded nor accelerated.

4.2. Co-Transport Experiments

Figure 3 presents the normalized effluent concentrations for FA and kaolinite (KGa-1b) colloids as function of pore volume for the simultaneous transport (co-transport) experiments of FA and KGa-1b in water unsaturated columns, at 4 different flow rates (1, 1.5, 2, and 3 mL/min). The M_r values were calculated with Equation (1) and are listed in Table 2. Note that the M_r values for FA were considerably lower in the presence than the absence of KGa-1b. Furthermore, the calculated $M_{1(\text{FA})}/M_{1(\text{tr})}$ ratio indicated that in the presence of KGa-1b the transport of FA was retarded by 23.7% at the lower flow rate (1 mL/min) and 14% at the higher flow rate (3 mL/min). The calculated $M_{1(\text{KGa-1b})}/M_{1(\text{tr})}$ ratio also indicated that KGa-1b was retarded by 50% at the lower flow rate (1 mL/min) and 1.6% at the higher flow rate (3 mL/min).

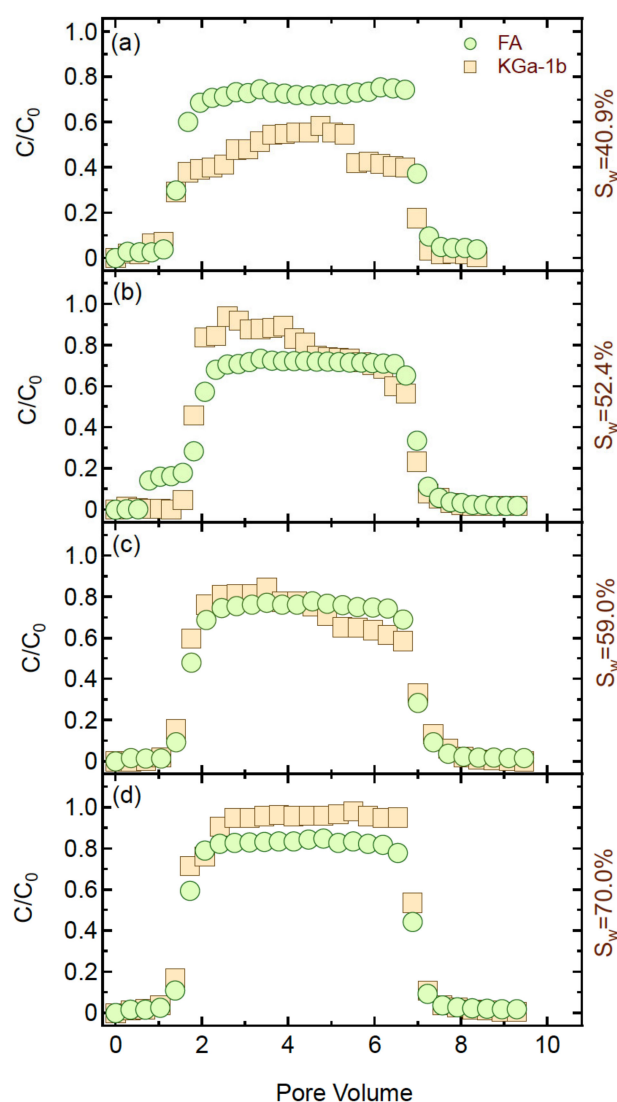


Figure 3. Breakthrough data from the co-transport experiments with FA and kaolinite particles in unsaturated columns packed with sand under various flow rates: (a) 1, (b) 1.5, (c) 2, and (d) 3 mL/min.

Figure 4 presents the normalized effluent concentrations for FA and montmorillonite (STx-1b) colloids as function of pore volume for the simultaneous transport (co-transport) experiments of FA and STx-1b in unsaturated columns, at 4 different flow rates (1, 1.5, 2, and 3 mL/min). The M_r values were determined with Equation (1) and are listed in Table 2. Note that the M_r values for FA were significantly lower in the presence than the absence of the STx-1b colloids. Furthermore, the calculated $M_{1(\text{FA})}/M_{1(\text{tr})}$ ratio indicated that in the presence of STx-1b the transport of FA was retarded for all flowrates used in this study (see Table 2). The calculated $M_{1(\text{STx-1b})}/M_{1(\text{tr})}$ ratio also indicated that STx-1b was retarded 22.6% at the lower flow rate (1 mL/min) and 4.7% at the higher flow rate (3 mL/min).

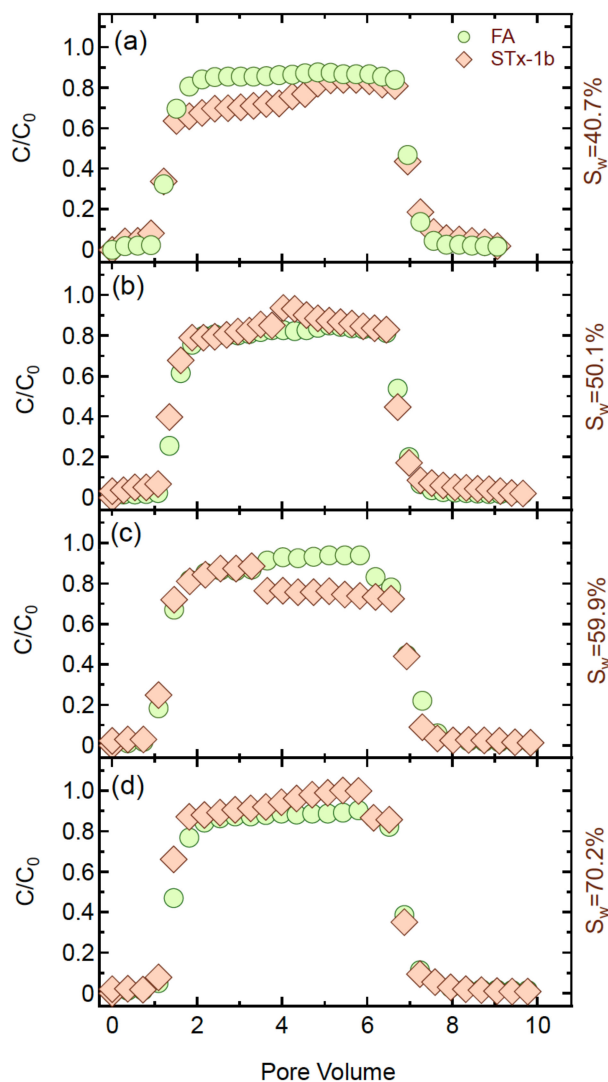


Figure 4. Breakthrough data from the co-transport experiments with FA and montmorillonite particles in unsaturated columns packed with sand under various flow rates: (a) 1, (b) 1.5, (c) 2, and (d) 3 mL/min.

Clearly, the experimental results suggested that both clay colloids (KGA-1b and STx-1b) hinder FA transport. In general, higher M_r values were observed for STx-1b than KGA-1b. The higher retention observed for KGA-1b could be attributed to its higher hydrophobicity compared to that of STx-1b. It should be noted that similar results have been reported in the literature by Syngouna and Chrysikopoulos [21]. Note that the maximum normalized FA concentrations in the effluent were in the range 0.97–1.00 in the absence of the clay colloids, 0.73–0.85 in the presence of KGA-1b, and 0.85–0.94 in the presence of STx-1b, suggesting that FA retention is proportional to clay retention (or inversely proportional to the clay M_r value).

The zeta potentials of KGA-1b and STx-1b colloids measured in the presence of FA were -36.8 ± 5.8 mV and -37.8 ± 3.0 mV, respectively. The zeta potential for the KGA-1b particles with and without formaldehyde was similar, but for STx-1b the zeta potential was more negative than in the absence of FA, probably due to FA adsorption onto STx-1b. Note that zeta potentials more negative than -30 mV suggest good stability.

The results of this study (see Table 2) clearly suggest that the presence of clay colloids hinder FA transport through unsaturated porous media. This is attributed to the retention of clay colloids in the porous medium, which in turn retain FA. Several theoretical and experimental investigations have shown that suspended mobile colloids can hinder the mobility of various contaminants in porous and

fractured porous media [62–65]. However, many other factors (e.g., changing pH and ionic strength, presence of organic matter, heterogeneity of natural soil), which are not examined in this study, could also affect the transport of FA in unsaturated porous media.

4.3. Collision Efficiencies

The experimental collision efficiency, a_{exp} , was calculated with Equation (2) for all co-transport cases considered in this study (see Table 2). The a_{exp} values for the co-transport experiments with KGa-1b were in general higher than those with ST_x-1b. The lower a_{exp} values were observed at the highest flow rate for both clay colloids (KGa-1b and ST_x-1b). This result is consistent with previously published experimental results [21,66,67]. According to filtration theory, a decrease in the interstitial velocity yields an increase in the number of collisions that occur between passive colloid particles and collectors, which eventually leads to increased colloid retention [67].

4.4. DLVO and Capillary Energy Profiles

Total Φ_{DLVO} interaction energy profiles, for the experimental conditions of this study, were determined for the interaction pairs for both clays (KGa-1b and ST_x-1b) with the two interfaces (AWI and SWI) and they are shown in Figure 5. The estimated minima (Φ_{min1} and Φ_{min2}) and energy barrier (Φ_{max1}) values are listed in Table 3. The DLVO interaction energy profiles indicate that Φ_{min1} exists only for the pair (ST_x-1b)-AWI (see Table 3). The absence of a negative Φ_{min1} suggests that permanent retention of clay colloids at AWI and SWI was unlikely to happen under the conditions of this study, whereas the existence of Φ_{min1} for the pair (ST_x-1b)-AWI suggests that ST_x-1b colloids could adhere onto AWIs if they possess sufficient kinetic energy to overcome the potential energy barrier. The inclusion of the Born repulsion contributed to the elimination of Φ_{min1} . Moreover, Φ_{min2} exists for the clay-SWI pairs considered here at very large separation distances ($h > 450$ nm). These are in accord with previously published experimental results [21]. Clearly, the DLVO theory suggests that clay attachment may occur on SWI only by ST_x-1b colloids, and that AWIs are not expected to retain clay colloids. It should be noted that similar results have been reported by Xu et al. [39]. However, the experimental results of this study showed that significant clay colloid retention occurred in the unsaturated column. Therefore, another retention mechanism must be involved. This deviation from DLVO predictions, can be explained by the presence of additional non-DLVO interactions, such as hydrophobic forces and hydration pressure [68]. These non-DLVO interactions may be stronger than van der Waals and double layer forces [42,60,69].

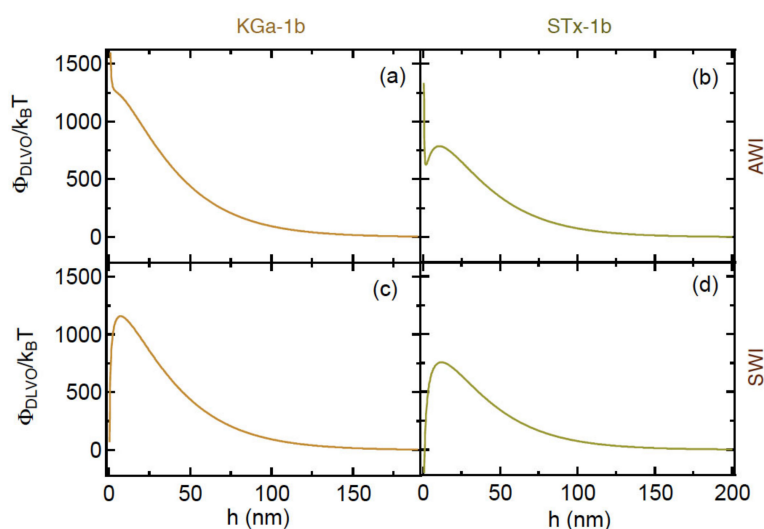


Figure 5. Predicted DLVO energy interactions as a function of separation distance, based on sphere-plate model for: (a) (KGa-1b)-AWI, (b) (ST_x-1b)-AWI, (c) (KGa-1b)-SWI, and (d) (ST_x-1b)-SWI.

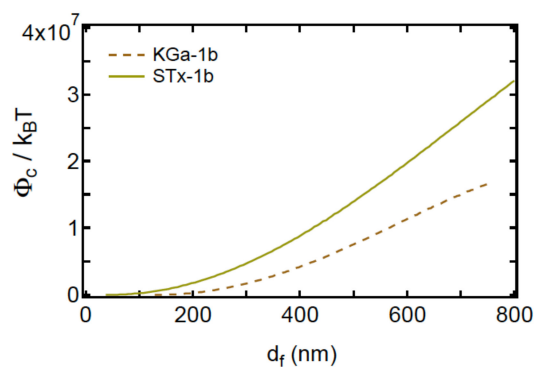
Table 3. Estimated Derjaguin-Landau-Verwey-Overbeek (DLVO) interaction energy profile components.

Interacting Pair	$\Phi_{\max 1}$ (k _B T)	$\Phi_{\min 1}$ (k _B T)	$\Phi_{\min 2}$ (k _B T)
(KGa-1b)-AWI	1278.9	na	na
(STx-1b)-AWI	788.2	na	na
(KGa-1b)-SWI	1160.9	na	−0.004
(STx-1b)-SWI	758.1	−958.5	−0.005

na: not available.

The DLVO theory has proven to be a useful tool for colloid transport and retention in unsaturated systems. However, previous research findings [60,68,69] suggested that DLVO theory does not always provide a good description of colloid interaction with the AWI. In unsaturated porous media, colloid retention is more complicated than in saturated porous media, due to the presence of AWIs. Non-DLVO interactions may occur on AWIs; however, they are neither fully understood nor yet quantified [68]. Bradford and Torkzaban [69] also reported that non-DLVO forces such as hydrophobic, hydro-dynamic and capillary forces are likely to play a significant role on colloid interactions with AWIs. This is consistent with the findings of this study where higher retention was observed for KGa-1b than ST_x-1b (KGa-1b is more hydrophobic than ST_x-1b).

The capillary energy potentials, Φ_c , of the clay colloids (KGa-1b and ST_x-1b), which were calculated as a function of distance d_f that a colloid protrudes out from a thin water film, are shown in Figure 6. The results are very similar to those reported by previous investigators [21,59,70]. As shown in Figure 6, the values of capillary energy potentials, Φ_c , are zero when the water film is thicker than or equal to the colloid diameter ($d_f \leq 0$), but they keep increasing as the colloid protrudes a distance $d_f > 0$ out of the water film. Note that the calculated capillary potential is lower for KGa-1b (the more hydrophobic clay colloid) than for ST_x-1b. Capillary energy forces are much greater than electric double layer repulsive forces and can push colloids close enough to the sand grains, and in turn lead to retention by van der Waals forces [21]. Moreover, attachment at the AWI interfaces is the responsible mechanism for the retention of both hydrophilic and hydrophobic colloids [26].

**Figure 6.** Effect of the distance d_f that a retained colloid protrudes a thin water film on the capillary potential energy, Φ_c , for clay colloids KGa-1b and ST_x-1b.

4.5. Effect of Water Saturation

The degree of saturation, S_w , and water content, θ_m , for the various experiments conducted in this study are listed in Table 2. Note that the breakthrough curves presented in Figure 2 show that the effluent FA concentrations are not affected by variations in water saturation. However, the results shown in Figures 3 and 4 for the co-transport experiments indicate that the breakthrough concentrations of FA and clay colloids are affected by the degree of saturation, which controls the water film thickness that leads to film straining [42]. The larger the water saturation, the higher the clay colloid peak concentration. Higher peak effluent concentrations are observed at larger flow rates (see $(C/C_0)_{\max}$ values in Table 2). Increased colloid mobilization, caused by increased flow rate and water

content, has also been reported by other investigators [58,71]. It should also be noted that a change in S_w may alter colloid retention due changes that occur in the hydrodynamic forces applied onto the colloids [48,65]. Previous studies have also demonstrated that colloid retention in porous media tends to be more pronounced when S_w is lowered [72].

5. Conclusions

The influence of two clay colloid particles (KGa-1b and ST_x-1b) on the transport of FA in unsaturated columns packed with quartz sand under various flow conditions was investigated. The results of this study show that the presence of kaolinite and montmorillonite colloids retarded by up to ~23% the transport of FA in unsaturated packed columns. In all cases considered in this study, the M_r values for FA were lower in the presence than the absence of clay particles. In most of the cotransport experiments, the M_r values for KGa-1b clay particles were lower than those for ST_x-1b clay particles, with M_r values ranging between 44.3% and 82.8% for KGa-1b, and 68.5% and 80.2% for ST_x-1b clay particles. DLVO interaction energy calculations demonstrated that permanent retention of clay colloids at air–water and solid water interfaces was insignificant, except for the pair (ST_x-1b)-SWI. However, the experimental results of this study showed that clay colloid retention occurred in the unsaturated column, especially at low flow rates. The retained colloids contributed to the increased FA retention. This deviation from DLVO predictions may be explained by the existence of additional non-DLVO forces (hydrophobic and capillary forces) that could be much stronger than van der Waals and double layer forces. Furthermore, the results of this study have shown that increasing the flow rate and water content leads to more pronounced colloid mobilization. The experimental findings of the present study improved our understanding of how clay colloid particles can affect the transport of FA in unsaturated porous media. The findings of this study not only advance the current knowledge of FA transport in unsaturated porous media, but also suggest that clay colloid particles could be used as adsorbents for the elimination of contaminants, such as FA, from waters by simple filtration.

Author Contributions: T.V.F. worked on the experimental design, collected, and analyzed the data, and wrote the first draft of the paper. C.V.C. supervised the research and contributed to the writing-reviewing and editing of the manuscript. All authors have read and agreed to the published version of the manuscript.

Funding: This research did not receive any specific grant from funding agencies in the public, commercial, or not-for-profit sectors.

Acknowledgments: The authors are thankful to R. Sarika for valuable laboratory assistance.

Conflicts of Interest: The authors declare that there is no conflict of interest.

Nomenclature

A_{123}	Hamaker constant (J), $M \cdot L^2/t^2$
C_{FA}	concentration of FA, M/L^3
C_{cc}	concentration of clay colloids, M/L^3
C_{FA-cc}	concentration of FA in the presence of clay colloids, M/L^3
C_{tr}	concentration of tracer, M/L^3
C_{iss}	concentration of colloid <i>i</i> at steady state, M/L^3
C_{i0}	influent colloid concentration, M/L^3
d_c	collector diameter, L
d_f	distance that a colloid protrudes out from a thin water film, L
d_p	average particle diameter, L
F_c	capillary force, $M \cdot L/t^2$
F_{pc}	parallel component of capillary force, $M \cdot L/t^2$
F_{vc}	vertical component of capillary force, $M \cdot L/t^2$
F_{v-tot}	total vertical capillary force, $M \cdot L/t^2$
g	gravitational acceleration, L/t^2
h	separation distance between two approaching surfaces, L

h_f	water film thickness, L
k_B	Boltzman's constant (J/K), $[M \cdot L^2 / t^2 \cdot T]$
m_0	total mass in the concentration breakthrough curve, $t \cdot M / L^3$
M_1	first normalized temporal moment, t
M_r	mass recovery, (-)
M_{in}	mass injected in the column, M / L^2
r_p	radius of colloidal particle, L
S_w	degree of saturation, (-)
T	temperature, K
U	interstitial fluid velocity, L/t
Greek letters	
a_{exp}	experimental collision efficiency, (-)
β	contact angle ($^\circ$)
η_0	single collector contact efficiency, (-)
θ	porosity (voids volume to porous medium volume), (-)
θ_m	volumetric water content (liquid volume to porous medium volume), (-)
μ_w	dynamic fluid viscosity, $M / L \cdot t$
ρ_p	colloidal particle density, M / L^3
ρ_f	fluid density, M / L^3
Φ_{Born}	Born potential energy (J), $M \cdot L^2 / t^2$
Φ_c	capillary potential energy (J), $M \cdot L^2 / t^2$
Φ_{dl}	electrostatic interaction energy (J), $M \cdot L^2 / t^2$
Φ_{DLVO}	DLVO potential energy (J), $M \cdot L^2 / t^2$
Φ_{max1}	primary maximum (J), $M \cdot L^2 / t^2$
Φ_{min1}	primary minimum (J), $M \cdot L^2 / t^2$
Φ_{min2}	secondary minimum (J), $M \cdot L^2 / t^2$
Φ_{vdW}	van der Waals potential energy (J), $M \cdot L^2 / t^2$
Abbreviations	
AWI	air–water interface
DLVO	Derjaguin-Landau-Verwey-Overbeek
ddH ₂ O	deionized distilled water
FA	Formaldehyde
KGa-1b	Kaolinite
STx-1b	Montmorillonite
SWI	Solid–water interface

References

- Denovio, N.M.; Sainers, J.E.; Ryan, J.N. Colloid movement in unsaturated porous media: Recent advances and future directions. *Vadose Zone J.* **2004**, *3*, 338–351. [[CrossRef](#)]
- Sen, T.K.; Khilar, K.C. Review on subsurface colloids and colloid-associated contaminant transport in saturated porous media. *Adv. Colloid Interface Sci.* **2006**, *119*, 71–96.
- De Jonge, L.W.; Kjaergaard, C.; Moldrup, P. Colloids and colloid-facilitated transport of contaminants in soils: An introduction. *Vadose Zone J.* **2004**, *3*, 321–325. [[CrossRef](#)]
- Grolimund, D.; Borkovec, M.; Barmettler, K.; Sticher, H. Colloid-facilitated transport of strongly sorbing contaminants in natural porous media: A laboratory column study. *Environ. Sci. Technol.* **1996**, *30*, 3118–3123. [[CrossRef](#)]
- Roy, S.B.; Dzombak, D.A. Chemical factors influencing colloid-facilitated transport of contaminants in porous media. *Environ. Sci. Technol.* **1997**, *31*, 656–664. [[CrossRef](#)]
- Wikiniyadhane, R.; Chotpanarat, S.; Ong, S.K. Effects of kaolinite colloids on Cd²⁺ transport through saturated sand under varying ionic strength conditions: Column experiments and modeling approaches. *J. Contam. Hydrol.* **2015**, *182*, 146–156. [[CrossRef](#)]

7. Wu, J.; Shen, C.; Wang, C.; Yan, A.; Zhang, H. The failure of using equilibrium adsorption of fosthiazate onto montmorillonite clay particles to predict their cotransport in porous media as revealed by batch and column studies. *J. Soils Sediments* **2019**, *19*, 917–928. [[CrossRef](#)]
8. Shen, C.; Wang, H.; Lazouskaya, V.; Du, Y.; Lu, W.; Wu, J.; Zhang, H.; Huang, Y. Cotransport of bismethiazol and montmorillonite colloids in saturated porous media. *J. Contam. Hydrol.* **2015**, *177–178*, 18–29. [[CrossRef](#)]
9. Xing, Y.; Chen, X.; Zhuang, J.; Chen, X. What happens when pharmaceuticals meet colloids. *Ecotoxicology* **2015**, *10*, 2100–2114. [[CrossRef](#)]
10. Maskaoui, K.; Zhou, J.L. Colloids as a sink for certain pharmaceuticals in the aquatic environment. *Environ. Sci. Pollut. Res.* **2009**, *17*, 898–907. [[CrossRef](#)]
11. Chen, H.; Gao, B.; Yang, L.Y.; Ma, L.Q. Montmorillonite enhanced ciprofloxacin transport in saturated porous media with sorbed ciprofloxacin showing antibiotic activity. *J. Contam Hydrol.* **2015**, *173*, 1–7. [[CrossRef](#)] [[PubMed](#)]
12. Vasiliadou, I.A.; Chrysikopoulos, C.V. Cotransport of *Pseudomonas putida* and kaolinite particles through water saturated columns packed with glass beads. *Water Resour. Res.* **2011**, *47*, W02543. [[CrossRef](#)]
13. Syngouna, V.I.; Chrysikopoulos, C.V. Cotransport of clay colloids and viruses in water saturated porous media. Colloids and Surfaces A: Physicochemical and Engineering Aspects. *Eng. Asp.* **2013**, *416*, 56–65. [[CrossRef](#)]
14. Syngouna, V.I.; Chrysikopoulos, C.V. Cotransport of clay colloids and viruses through water-saturated vertically oriented columns packed with glass beads: Gravity effects. *Sci. Total. Environ.* **2016**, *545–546*, 210–218. [[CrossRef](#)]
15. Syngouna, V.I.; Chrysikopoulos, C.V.; Kokkinos, P.; Tselepi, M.A.; Vantarakis, A. Cotransport of human adenoviruses with clay colloids and TiO₂ nanoparticles in saturated porous media: Effect of flow velocity. *Sci. Total Environ.* **2017**, *598*, 160–167. [[CrossRef](#)]
16. Katzourakis, V.E.; Chrysikopoulos, C.V. Mathematical modeling of colloid and virus cotransport in porous media: Application to experimental data. *Adv. Water Resour.* **2014**, *68*, 62–73. [[CrossRef](#)]
17. Molnar, I.L.; Johnson, W.P.; Gerhard, J.L.; Willson, C.S.; O'Carroll, D.M. Predicting colloid transport through saturated porous media: A critical review. *Water Resour. Res.* **2015**, *51*, 6804–6845. [[CrossRef](#)]
18. Li, X.; Zhang, W.; Qin, Y.; Ma, T.; Zhou, J.; Du, S. Fe-colloid cotransport through saturated porous media under different hydrochemical and hydrodynamic conditions. *Sci. Total Environ.* **2019**, *647*, 494–506. [[CrossRef](#)]
19. Knappenberger, T.; Flury, M.; Mattson, E.D.; Harsh, J.B. Does water content or flow rate control colloid transport in unsaturated porous media? *Environ Sci Technol.* **2014**, *48*, 3791–3799. [[CrossRef](#)]
20. Cheng, T.; Saiers, J.E. Colloid-facilitated transport of cesium in vadose-zone sediments: The importance of flow transients. *Environ. Sci. Technol.* **2010**, *44*, 7443–7449. [[CrossRef](#)]
21. Syngouna, V.I.; Chrysikopoulos, C.V. Experimental investigation of virus and clay particles cotransport in partially saturated columns packed with glass beads. *J. Colloid Interf. Sci.* **2015**, *440*, 140–150. [[CrossRef](#)] [[PubMed](#)]
22. Sirivithayapakorn, S.; Keller, A. Transport of colloids in unsaturated porous media: A pore-scale observation of processes during the dissolution of air-water interface. *Water Resour. Res.* **2003**, *39*, 1346. [[CrossRef](#)]
23. Ghanbarian-Alavijeh, B.; Skinner, T.E.; Hunt, A.G. Saturation dependence of dispersion in porous media. *Phys. Rev. E* **2012**, *86*, 066316. [[CrossRef](#)] [[PubMed](#)]
24. Flury, M.; Aramrak, S. Role of air-water interfaces in colloid transport in porous media: A review. *Water Resour. Res.* **2017**, *53*, 5247–5275. [[CrossRef](#)]
25. Wan, J.; Tokunaga, T.K. Film straining of colloids in unsaturated porous media: Conceptual model and experimental testing. *Environ. Sci. Technol.* **1997**, *31*, 2413–2420. [[CrossRef](#)]
26. Crist, J.T.; Zevi, Y.; McCarthy, J.F.; Throop, J.A.; Steenhuis, T.S. Transport and retention mechanisms of colloids in partially saturated porous media. *Vadose Zone J.* **2005**, *4*, 184–195. [[CrossRef](#)]
27. Sim, Y.; Chrysikopoulos, C.V. Virus transport in unsaturated porous media. *Water Resour. Res.* **2000**, *36*, 173–179. [[CrossRef](#)]
28. Baumann, T.; Fruhstorfer, P.; Klein, T.; Niessner, R. Colloid and heavy metal transport at landfill sites in direct contact with groundwater. *Water Res.* **2006**, *40*, 2776–2786. [[CrossRef](#)]
29. Chotpantararat, S.; Kiatvarangkul, N. Facilitated transport of cadmium with montmorillonite KSF colloids under different pH conditions in water-saturated sand columns: Experiment and transport modeling. *Water Res.* **2018**, *146*, 216–231. [[CrossRef](#)]

30. Yuan, H.; Li, G.; Yang, L.; Yan, X.; Yang, D. Development of melamine formaldehyde resin microcapsules with low formaldehyde emission suited for seed treatment. *Colloids Surfaces B Biointerfaces* **2015**, *128*, 149–154. [[CrossRef](#)]
31. Nash, T. The colorimetric estimation of formaldehyde by means of the Hantzsch reaction. *Biochem. J.* **1953**, *55*, 416–421. [[CrossRef](#)] [[PubMed](#)]
32. Fountouli, T.V.; Chrysikopoulos, C.V.; Tsanis, I.K. Effect of salinity on formaldehyde interaction with quartz sand and kaolinite colloid particles: Batch and column experiments. *Environ. Earth Sci.* **2019**, *78*, 152. [[CrossRef](#)]
33. Seyfioglu, R.; Odabasi, M.; Cetin, E. Wet and dry deposition of formaldehyde in Izmir, Turkey. *Sci. Total Environ.* **2006**, *366*, 809–818. [[CrossRef](#)] [[PubMed](#)]
34. Economou, C.; Mihalopoulos, N. Formaldehyde in the rainwater in the eastern Mediterranean: Occurrence, deposition and contribution to organic carbon budget. *Atmos. Environ.* **2002**, *36*, 1337–1347. [[CrossRef](#)]
35. Syngouna, V.I.; Chrysikopoulos, C.V. Transport of biocolloids in water saturated columns packed with sand: Effect of grain size and pore water velocity. *J. Contam. Hydrol.* **2011**, *126*, 301–314. [[CrossRef](#)]
36. Fountouli, T.V.; Chrysikopoulos, C.V. Adsorption and thermodynamics of pharmaceuticals, acyclovir and fluconazole, onto quartz sand under static and dynamic conditions. *Environ. Eng. Sci.* **2018**, *35*, 909–917. [[CrossRef](#)]
37. Chrysikopoulos, C.V.; Sotirelis, N.P.; Kallithrakas-Kontos, N.G. Cotransport of graphene oxide nanoparticles and kaolinite colloids in porous media. *Transp. Porous Media* **2017**, *119*, 181–204. [[CrossRef](#)]
38. Rong, X.; Huang, Q.; He, X.; Chen, H.; Cai, P.; Liang, W. Interaction of *Pseudomonas putida* with kaolinite and montmorillonite: A combination study by equilibrium adsorption, ITC, SEM and FTIR. *Colloids Surf. B* **2008**, *64*, 49–55. [[CrossRef](#)]
39. Xu, S.; Qi, J.; Chen, X.; Lazouskay, V.; Zhuang, J.; Jin, Y. Coupled effect of extended DLVO and capillary interactions on the retention and transport of colloids through unsaturated porous media. *Sci. Total Environ.* **2016**, *573*, 564–572. [[CrossRef](#)]
40. El-Farhan, Y.H.; Denovio, N.M.; Herman, J.S.; Hornberger, G.M. Mobilization and transport of soil particles during infiltration experiments in an agricultural field, Shenandoah Valley, Virginia. *Environ. Sci. Technol.* **2000**, *34*, 3555–3559. [[CrossRef](#)]
41. Anders, R.; Chrysikopoulos, C.V. Transport of viruses through saturated and unsaturated columns packed with sand. *Transp. Porous Media* **2009**, *76*, 121–138. [[CrossRef](#)]
42. Mitropoulou, P.N.; Syngouna, V.I.; Chrysikopoulos, C.V. Transport of colloids in unsaturated packed columns: Role of ionic strength and sand grain size. *J. Chem. Eng.* **2013**, *232*, 237–248. [[CrossRef](#)]
43. Lewis, J.; Sjöström, J. Optimizing the experimental design of soil columns in saturated and unsaturated transport experiments. *J. Contam. Hydrol.* **2010**, *115*, 1–13. [[CrossRef](#)] [[PubMed](#)]
44. Chrysikopoulos, C.V. Artificial tracers for geothermal reservoir studies. *Environ. Geology* **1993**, *22*, 60–70.
45. James, S.C.; Chrysikopoulos, C.V. Monodisperse and polydisperse colloid transport in water-saturated fractures with various orientations: Gravity effects. *Adv. Water Resour.* **2011**, *34*, 1249–1255. [[CrossRef](#)]
46. Chrysikopoulos, C.V.; Katzourakis, V.E. Colloid particle size-dependent dispersivity. *Water Resour. Res.* **2015**, *51*, 4668–4683. [[CrossRef](#)]
47. Saiers, J.E.; Lenhart, J.J. Colloid mobilization and transport within unsaturated porous media under transient-flow conditions. *Water Resour. Res.* **2003**, *39*, 1019. [[CrossRef](#)]
48. Tufenkji, N.; Elimelech, M. Correlation equation for predicting single-collector efficiency in physicochemical filtration in saturated porous media. *Environ. Sci. Technol.* **2004**, *38*, 529–536. [[CrossRef](#)]
49. Van Olphen, H.; Fripiat, J.J. *Data Handbook for Clay Minerals and Other Non-Metallic Minerals*; Pergamon Press: Oxford, UK, 1979.
50. Chrysikopoulos, C.V.; Syngouna, V.I. Attachment of bacteriophages MS2 and Φ X174 onto kaolinite and montmorillonite: Extended-DLVO interactions. *Colloids Surfaces B Biointerfaces* **2012**, *92*, 74–83. [[CrossRef](#)]
51. Verwey, E.J.W.; Overbeek, J.T.G. *Theory of the Stability of Lyophobic Colloids: The Interaction of Sol Particles Having an Electric Double Layer*; Elsevier: Amsterdam, The Netherlands, 1948.
52. Hogg, R.; Healy, T.W.; Fuerstenau, D.W. Mutual coagulation of colloidal dispersions. *Trans. Faraday Soc.* **1966**, *62*, 1638–1651. [[CrossRef](#)]
53. Loveland, J.P.; Ryan, J.N.; Amy, G.L.; Harvey, R.W. The reversibility of virus attachment to mineral surfaces. *Colloids Surfaces A Physicochem. Eng. Asp.* **1996**, *107*, 205–221. [[CrossRef](#)]

54. Gregory, J. Approximate expressions for retarded van der Waals interaction. *J. Colloid Interface Sci.* **1981**, *83*, 138–145. [[CrossRef](#)]
55. Ruckenstein, E.; Prieve, D.C. Adsorption and desorption of particles and their chromatographic separation. *AIChE J.* **1976**, *22*, 276–283. [[CrossRef](#)]
56. Israelachvili, J.N. *Intermolecular and Surface Forces 2011*, 3rd ed.; Academic Press: London, UK, 2011.
57. Novich, B.E.; Ring, T.A. Colloid stability of clays using photon correlation spectroscopy. *Clays Clay Miner.* **1984**, *32*, 400–406. [[CrossRef](#)]
58. Shang, J.; Flury, M.; Chen, G.; Zhuang, J. Impact of flow rate, water content, and capillary forces on in situ colloid mobilization during infiltration in unsaturated sediments. *Water Resour. Res.* **2008**, *44*, W06411. [[CrossRef](#)]
59. Gao, B.; Steenhuis, T.S.; Zevi, Y.; Morales, V.L.; Nieber, J.L.; Richards, B.K.; McCarthy, J.F.; Parlange, J.-Y. Capillary retention of colloids in unsaturated porous media. *Water Resour. Res.* **2008**, *44*, W04504. [[CrossRef](#)]
60. Bai, H.; Cochet, N.; Pauss, A.; Lamy, E. DLVO, hydrophobic, capillary and hydrodynamic forces acting on bacteria at solid-air-water interfaces: Their relative impact on bacteria deposition mechanisms in unsaturated porous media. *Colloids Surf. B Biointerfaces* **2017**, *150*, 41–49. [[CrossRef](#)]
61. Wu, W. Baseline studies of the clay minerals society source clays: Colloid and surface phenomena. *Clays Clay Miner.* **2001**, *49*, 446–452. [[CrossRef](#)]
62. Abdel-Salam, A.; Chrysikopoulos, C. Modeling of colloid and colloid-facilitated contaminant transport in a two-dimensional fracture with spatially variable aperture. *Transport Porous Media* **1995**, *20*, 197–221. [[CrossRef](#)]
63. Abdel-Salam, A.; Chrysikopoulos, C. Analysis of a model for contaminant transport in fractured media in the presence of colloids. *J. Hydrol.* **1995**, *165*, 261–281. [[CrossRef](#)]
64. Katzourakis, V.E.; Chrysikopoulos, C.V. Modeling dense-colloid and virus cotransport in three-dimensional porous media. *J. Contam. Hydrol.* **2015**, *181*, 102–113. [[CrossRef](#)] [[PubMed](#)]
65. Won, J.; Wirth, X.; Burns, S.E. An experimental study of cotransport of heavy metals with kaolinite colloids. *J. Hazard. Mater.* **2019**, *373*, 476–482. [[CrossRef](#)] [[PubMed](#)]
66. Pang, L. Microbial removal rates in subsurface media estimated from published studies of field experiments and large intact soil cores. *J. Environ. Qual.* **2009**, *38*, 1531–1559. [[CrossRef](#)] [[PubMed](#)]
67. Walshe, G.E.; Pang, L.; Flury, M.; Close, M.E.; Flintoft, M. Effects of pH, ionic strength, dissolved organic matter, and flow rate on the co-transport of MS2 bacteriophages with kaolinite in gravel aquifer media. *Water Res.* **2010**, *44*, 1255–1269. [[CrossRef](#)]
68. Grasso, D.; Subramaniam, K.; Butkus, M.; Strevett, K.; Bergendahl, J. A review of non-DLVO interactions in environmental colloidal systems. *Rev. Environ. Sci. Biotechnol.* **2002**, *1*, 17–38. [[CrossRef](#)]
69. Bradford, S.A.; Torkzaban, S. Colloid transport and retention in unsaturated porous media: A review of interface-, collector-, and pore-scale processes and models. *Vadose Zone J.* **2008**, *7*, 667–681. [[CrossRef](#)]
70. Zevi, Y.; Dathe, A.; McCarthy, J.F.; Richards, B.K.; Steenhuis, T.S. Distribution of colloid particles onto interfaces in partially saturated sand. *Environ. Sci. Technol.* **2005**, *39*, 18. [[CrossRef](#)]
71. Gao, B.; Saiers, J.E.; Ryan, J.N. Deposition and mobilization of clay colloids in unsaturated porous media. *Water Resour. Res.* **2004**, *40*, W08602. [[CrossRef](#)]
72. Liu, L.; Gao, B.; Wu, L.; Morales, V.L.; Yang, L.; Zhou, Z.; Wang, H. Deposition and transport of graphene oxide in saturated and unsaturated porous media. *Chem. Eng. J.* **2013**, *229*, 444–449. [[CrossRef](#)]

Publisher's Note: MDPI stays neutral with regard to jurisdictional claims in published maps and institutional affiliations.



© 2020 by the authors. Licensee MDPI, Basel, Switzerland. This article is an open access article distributed under the terms and conditions of the Creative Commons Attribution (CC BY) license (<http://creativecommons.org/licenses/by/4.0/>).